Applied Catalysis B: Environmental 162 (2015) 544–550

Contents lists available at ScienceDirect

Applied Catalysis B: Environmental

journal homepage: www.elsevier.com/locate/apcatb

Investigation on microwave absorbing properties of loaded $MnFe_2O_4$ and degradation of Reactive Brilliant Red X-3B

Xue Fang, Jun Xiao, Shaogui Yang*, Huan He, Cheng Sun

State Key Laboratory of Pollution Control and Resource Reuse, School of the Environment, Nanjing University, Nanjing 210023, PR China

ARTICLE INFO

Article history:
Received 23 March 2014
Received in revised form 13 June 2014
Accepted 10 July 2014
Available online 18 July 2014

Keywords:
Loaded manganese ferrite
Microwave absorbing property
Dye degradation
Microtoxicity

ABSTRACT

Four nanocomposite catalysts namely $MnFe_2O_4$, $MnFe_2O_4$-SiC, $MnFe_2O_4$-TiO_2 and $MnFe_2O_4$-diatomite, were synthesized and characterized by X-ray diffraction (XRD) and N_2 adsorption (BET specific surface area). Measurements of the catalysts' complex permittivity and permeability in the microwave (MW) frequency range of 0.5–18 GHz showed $MnFe_2O_4$-SiC composites to be the best MW absorbers. The surface temperature of $MnFe_2O_4$-SiC (1450 °C) under MW was higher compared to those of the other three catalysts, indicating that silicon carbide (SiC) was an effective support. MW-assisted experiments demonstrated that the degradation of RBR X-3B with $MnFe_2O_4$-SiC reached 92%, achieved 70% of TOC removal and exhibited lower toxicity with 5 min MW irradiation, proving $MnFe_2O_4$-SiC to be an excellent microwave catalyst. These findings are important regarding the development of efficient sorbents that are effective microwave absorbers as well as catalysts of rapid degradation of pollutants.

1. Introduction

Microwave (MW) technique has been applied in various fields, such as organic synthesis [1,2], analysis [3], military and environmental engineering [4,5]. Researches described in [6–8] have focused on the application of MW irradiation in environmental wastewater treatment, particularly in the degradation of azo-dyes with complex aromatic structures, which are toxic and nondegradable [9,10]. The microwave-assisted degradation technique for pollutants can potentially reduce reaction time and save energy [11].

Over the past decade, MW absorbing materials, known as dielectrics, have been the focus of much attention, particularly for their significant roles in wastewater treatment. Materials, such as activated carbon [12,13], metallic powders [14,15], CNTs [16,17] and polymers [18], are commonly used in microwave-assisted degradation of organic pollutants. Among MW absorbents, ferrites (MFe_2O_4) are the most promising [19]. Depending on the chemical properties of M^{2+} and Fe^{3+} which occupy the tetrahedral and octahedral interstitial sites in the nanoscale MFe_2O_4 [20], the nanocrystalline ferrites present high magnetic permeability or electrical resistivity. However, the nanoscale MFe_2O_4 can be easily lost during degradation, resulting in lower efficiency and stability. To resolve this drawback, the smaller higher-activity particles of MFe_2O_4 can be scattered to the supports [21]. Meanwhile, due to what has been broadly termed "hot-spot effects", MW energy can be transferred rapidly from the low-loss supports to the azo-dyes [22]. It is reasonable to suggest that under MW irradiation the coated MFe_2O_4 can demonstrate remarkable catalytic activity. However, it can be theoretically assumed that different supports will impact in different ways on the catalytic activity of the coated MFe_2O_4. Coated composites have been reported in literature [5,16], but the influence of different supports on ferrites concerning degradation of pollutants has not been investigated yet.

$MnFe_2O_4$, which can be easily prepared and is of low cost, has been applied in absorption of organic pollutants [23]. However, in the field of MW-assisted degradation, little report has been investigated. In this study, $MnFe_2O_4$ and its coated composites ($MnFe_2O_4$-SiC, $MnFe_2O_4$-TiO_2 and $MnFe_2O_4$-diatomite) were prepared and used to degrade the commercial azo-dyes under microwave irradiation. Reactive Brilliant Red X-3B (RBR X-3B) which is a kind of typical azo-dye was chosen as a representative target compound. The MW absorbing performance parameters of the four catalysts and their catalytic capacities were compared and discussed systematically. In addition, extensive work has been carried out to evaluate the toxicity of the target compound before and after degradation based on the bioluminescence test. The main objective of this study is to investigate the influence of various supports have over ferrites regarding degradation of pollutants, to explore the cause of different catalytic performances, and to

* Corresponding author. Tel.: +86 25 89680580; fax: +86 25 89680580.
E-mail addresses: yangsg@nju.edu.cn, yangdlut@126.com (S. Yang).

http://dx.doi.org/10.1016/j.apcatb.2014.07.022
0926-3373/

identify the optimal MW catalyst which can be applied in the degradation of azo-dyes in conjunction with MW irradiation technology.

2. Experimental materials and methods

2.1. Reagents and materials

$Fe(NO_3)_3$, $Mn(NO_3)_2$, NaOH and HCl were provided by Nanjing Chemical Company. Silicon carbide (SiC) and diatomite (SiO_2) were purchased from Beijing Daoking Company (Beijing, China). Tetrabutyl titanate, cetyltrimethylammonium bromide (CTAB), anhydrous ethanol, *n*-butanol, tert-butyl alcohol and $Na_2C_2O_4$ were from Sinopharm Chemical Reagent Co. Ltd. (Shanghai, China). Reactive Brilliant Red X-3B was obtained from Sigma Company. The water used throughout the study was deionized. All the other chemicals were of analytical grade. Stock solution was prepared by dissolving measured amount of dyes in pure water.

The chemical structure of RBR X-3B is as follows:

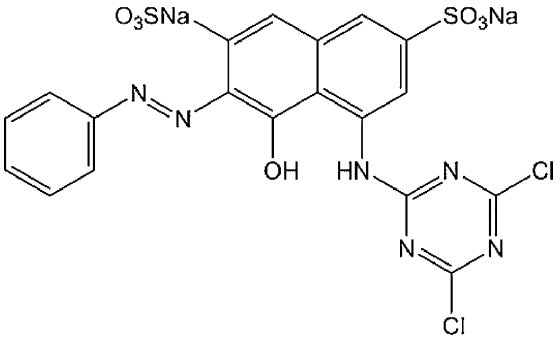

2.2. Preparation of $MnFe_2O_4$ nanoparticles

The $MnFe_2O_4$ powders were synthesized by using the hydrothermal method. The $Fe(NO_3)_3$ and $Mn(NO_3)_2$ salts (molar ratio of Fe:Mn = 2:1) were dissolved in 100 mL pure water. A few drops of NaOH (0.1 M) were gently added to the solutions to adjust its pH to 11; the solution was then stirred for 2 h at 75 °C. Following this, the coprecipitations and solutions were transferred to the high pressure kettles. After heating at 180 °C for 12 h, the solutions were filtrated and washed with deionized water to get the as-prepared $MnFe_2O_4$ powders. When the powders were dried at 50 °C for 6 h, and calcined at 700 °C for 2 h in air, the nano-$MnFe_2O_4$ powders were obtained.

2.3. Preparation of coated $MnFe_2O_4$ nanoparticles

2.3.1. Preparation of $MnFe_2O_4$-TiO_2

The whole preparation was carried out in an ultrasonic wave pool (40 kHz and 240 W) [24]. In the experiment, the as-prepared $MnFe_2O_4$ and CTAB (mass ratio 1:1) were dissolved into anhydrous ethanol and *n*-butanol (volume ratio 1:8). When drops of HCl solution (2 wt.%) were added to the solution, the mixture was sonicated for 30 min. Then, tetrabutyloxide titanium (0.1 M) was added into the mixture to sonicate for 4 h. The precipitates were separated, washed repeatedly with anhydrous ethanol and dried in air. After being calcined at 700 °C for 2 h, the $MnFe_2O_4$-TiO_2 composites were obtained. The weight content of TiO_2 in $MnFe_2O_4$-TiO_2 was 50%.

2.3.2. Preparation of $MnFe_2O_4$-SiC and $MnFe_2O_4$-diatomite

The $MnFe_2O_4$-SiC (or diatomite) powders were synthesized by the sol–gel method. $Fe(NO_3)_3$ and $Mn(NO_3)_2$ salts (molar ratio of Fe:Mn = 2:1) were dissolved in 100 mL pure water. After the solutions were stirred for 30 min at 60 °C, citric acid was added. The solutions were then heated up to 80 °C and stirred for 2 h. After that, SiC (or diatomite) powders were added to the mixtures. Heated at 80 °C for 4 h, the mixed solutions were dried to form the precursors. Then, the precursors were dried at 120 °C for 10 h and calcined at 700 °C for 2 h to obtain the $MnFe_2O_4$-SiC (or diatomite) powders. The weight content of SiC (or diatomite) in $MnFe_2O_4$-SiC (or diatomite) was 50%.

2.4. Characterization

The X-ray diffraction (XRD) analysis was carried out on an X-ray diffractometer (Shimadzu LabX XRD-6000, Cu KR radiation). The specific surface areas of the samples were analyzed by N_2-BET analyzer ASAP 2020.

To measure the microwave properties, the samples were dispersed into paraffin wax (volume ratio of composites: 60%). The outer and inner diameters of the testing specimens were 7.0 and 3.0 mm respectively, with a thickness of 2.0 mm. ε', ε'', μ', μ'' of the samples were measured by using an Agilent vector network analyzer within the range of 0.5–18 GHz. The absorbing properties (reflection losses: RL) were calculated in Matlab 7.0 with the following equations [25]:

$$\mathrm{RL}\ \ (\mathrm{dB}) = 20\log_{10}\left|\frac{z_{in}-1}{z_{in}+1}\right| \tag{1}$$

$$z_{in} = \left(\frac{\mu_r}{\varepsilon_r}\right)^{1/2}\tanh\left[j\left(\frac{2\pi fd}{C}\right)(\mu_r\varepsilon_r)^{1/2}\right] \tag{2}$$

where z_{in} is the normalized input impedance with free space, $\varepsilon_r = \varepsilon' - j\varepsilon''$ and $\mu_r = \mu' - j\mu''$ are the complex relative permeability and permittivity of the samples, d represents the thickness of the absorber, C and f are the velocity of light and the frequency of the microwave in the free space, respectively. RL versus frequency can be calculated at a specified thickness from ε_r and μ_r.

2.5. Investigation on the temperature of the samples under MW irradiation

In order to determine the variational temperature under MW irradiation, 0.15 g of $MnFe_2O_4$, $MnFe_2O_4$-TiO_2, $MnFe_2O_4$-SiC and $MnFe_2O_4$-diatomite were put into a quartz tube [26], and then irradiated by microwave oven. Meanwhile, the surface temperatures of catalysts were measured by the Optris infrared thermometers (Germany, CT G5) which embedded in the microwave oven.

2.6. MW degradation of RBR X-3B

For the microwave catalytic degradation, a microwave oven (800 W, 2.45 GHz) was selected. 100 mL of RBR X-3B solution (20 mg L^{-1}) and 0.15 g catalysts ($MnFe_2O_4$, $MnFe_2O_4$-TiO_2, $MnFe_2O_4$-SiC and $MnFe_2O_4$-diatomite) were added into the 250 mL glass reactor for each. After degradation, the catalysts were separated by a magnet for the reason that the catalysts exhibited strong magnetism. The liquid supernatant was sampled at various times to measure the degradation efficiencies of RBR X-3B by UV–vis spectra (Shimadzu, 2550, Japan), whose maximal absorbing wavelength is 537 nm. The standard curve of RBR X-3B was shown in Fig. S1 (detection limit: 0.016 mg L^{-1}). The degradation percentages were calculated by the following equation:

$$\mathrm{Removal}\ \ (\%) = \frac{C_0 - C_t}{C_0}\times 100 \tag{3}$$

where C_0 represents the initial concentration and C_t is the concentration at time t.

Total organic carbon (TOC) of the RBR X-3B solutions during the degradation was analyzed by TOC-5000A analyzer (Shimadzu Japan).

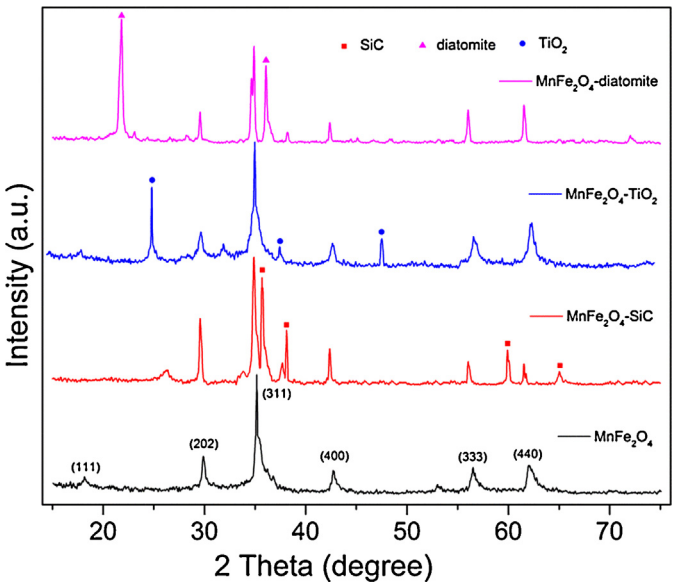

Fig. 1. XRD diffraction patterns of synthesized $MnFe_2O_4$, $MnFe_2O_4$-SiC, $MnFe_2O_4$-TiO_2 and $MnFe_2O_4$-diatomite.

2.7. Bioluminescence test

To evaluate the variation of toxicity during degradation, the bioluminescence test was applied to the samples at various treatment times. The changes of acute toxicity based on the inhibition of the bioluminescence of *Photobacterium phosphoreum* [27,28] were compared during degradation. The tests were conducted according to the Chinese standard GB/T15441-1995. After 30 min incubation, the solutions were measured in Luminometer DXY-2 (Nanjing Soil Institute of Chinese Academy of Sciences).

3. Results and discussion

3.1. XRD analysis

The XRD patterns of $MnFe_2O_4$ and three coated $MnFe_2O_4$ are displayed in Fig. 1 where the sharp intensive peaks at $2\theta = 29.59$, 34.88, 42.40, 56.02 and 61.52, which are the characteristic peaks of $MnFe_2O_4$, JCPDS card (no. 38-0430), can be observed. Meanwhile, the diffraction patterns consistent with SiC (no. 49-1428), TiO_2 (no. 21-1272) and diatomite (no. 39-1425) were observed in the coated $MnFe_2O_4$, indicating that $MnFe_2O_4$ was coated successfully in the surfaces of SiC, TiO_2 and diatomite, respectively. According to Scherrer's equation, the sizes of $MnFe_2O_4$-SiC, $MnFe_2O_4$-TiO_2, $MnFe_2O_4$-diatomite and $MnFe_2O_4$ were calculated to be 22.87, 27.50, 41.20 and 31.67 nm, respectively. The differences of composite sizes result from the different supports on $MnFe_2O_4$, which may lead to different chemical properties. For instance, the contact areas between smaller particles and the dye molecules were larger, which could promote the degradation processes.

3.2. Specific surface area – N_2 adsorption

Nitrogen adsorption/desorption isotherms of the four catalysts are presented in Fig. 2. A wide hysteresis area of N_2 adsorption/desorption isotherms could be viewed when it comes to the composites, especially for $MnFe_2O_4$-SiC and $MnFe_2O_4$-TiO_2. This suggests that the pores are distributed widely enough [29,30], as is shown by the insets in each figure. The specific surface areas were 17.40, 50.13, 120.83 and 5.41 $m^2\,g^{-1}$ for $MnFe_2O_4$, $MnFe_2O_4$-TiO_2, $MnFe_2O_4$-SiC and $MnFe_2O_4$-diatomite, respectively. Interestingly, S_{BET} increases considerably with the addition of SiC or TiO_2, which is due to the good adsorptions of the supports introduced. The addition of support has been significant in increasing the specific surface area, an increase which according to Yuan et al. [31] could result in a better catalytic performance.

3.3. Dielectric and magnetic parameters

The variations of the relative permittivity and permeability of the four catalysts with the frequencies are shown in Fig. 3. It is widely accepted that the MW absorption properties of the materials are determined by the complex permittivity ($\varepsilon' - j\varepsilon''$) and permeability ($\mu' - j\mu''$). Hence, optimizing the complex relative permittivity and permeability has a direct effect on and can change the materials' MW absorbing ability. The real and the imaginary parts of the relative permittivity ε' and ε'' in $MnFe_2O_4$-TiO_2, $MnFe_2O_4$ and $MnFe_2O_4$-diatomite are almost constant. However, the real and imaginary parts ε' and ε'' in $MnFe_2O_4$-SiC are much larger than those in the other three catalysts, which indicate that $MnFe_2O_4$-SiC composites exhibit high dielectric loss [32]. In addition, the real and imaginary parts of the relative permeability μ' and μ'' in $MnFe_2O_4$-TiO_2, $MnFe_2O_4$ and $MnFe_2O_4$-diatomite are positive, while the μ'' in $MnFe_2O_4$-SiC is negative, indicating that the magnetic loss of $MnFe_2O_4$-SiC is extremely low. The dielectric/magnetic loss tangents with the frequency of the four catalysts calculated by $\tan\delta_e = \varepsilon''/\varepsilon'$ and $\tan\delta_\mu = \mu''/\mu'$ are shown in Fig. 4. It is observed that the value of the dielectric loss is much larger than the magnetic loss in $MnFe_2O_4$-SiC, suggesting that the MW absorption originates from the dielectric loss [33]. For $MnFe_2O_4$-TiO_2, the value of dielectric loss is higher than the value of magnetic loss. In contrast, the MW absorption of $MnFe_2O_4$ is attributed to the magnetic loss. Moreover, both the dielectric and magnetic loss in $MnFe_2O_4$–diatomite are smaller, leading to poor microwave absorption.

3.4. Microwave absorbing properties

According to Eqs. (1) and (2), the surface reflectivity of the material is a function of six characteristics parameters: ε', ε'', μ', μ'', f and d. Fig. 5 represents the variations of the reflectivity for the four catalysts in the frequency range of 0.5–18 GHz, with the matching thickness of 3.5 mm. It can be observed that the bandwidths of the reflection loss at −5 dB are 0.9 (curve *a*), 5.03 (curve *b*), 1.88 (curve *c*) GHz, respectively. $MnFe_2O_4$-SiC composites achieve the maximum absorbing value of −11.5 dB at 2.69 GHz (curve a), and the bandwidth of the reflection loss at −10 dB is 0.3 GHz. In fact, 90% of power is absorbed by the catalyst with respect to −10 dB reflection loss, while 70% of power absorption is achieved when it comes to −5 dB loss [33,34]. The lower the value of reflection loss is, the poorer the microwave absorbing properties are. As seen in Fig. 5, the order of reflection loss is $MnFe_2O_4$-SiC > $MnFe_2O_4$-TiO_2 > $MnFe_2O_4$ > $MnFe_2O_4$-diatomite. It is evident that $MnFe_2O_4$-SiC exhibits a high value of reflection loss, which is the result of a larger permittivity. As it has been reported in literature [16,19], the reflection loss of the catalysts with large particles is extremely low, resulting in a poor MW absorption. Herein, the initial particle sizes strongly affect the complex permeability, permittivity and further the MW absorbing properties. The smaller particles with the larger surface area, such as $MnFe_2O_4$-SiC, could enhance the space-charge polarization between the metal ions to improve the value of permittivity, corresponding to the analysis of characterization by XRD and BET.

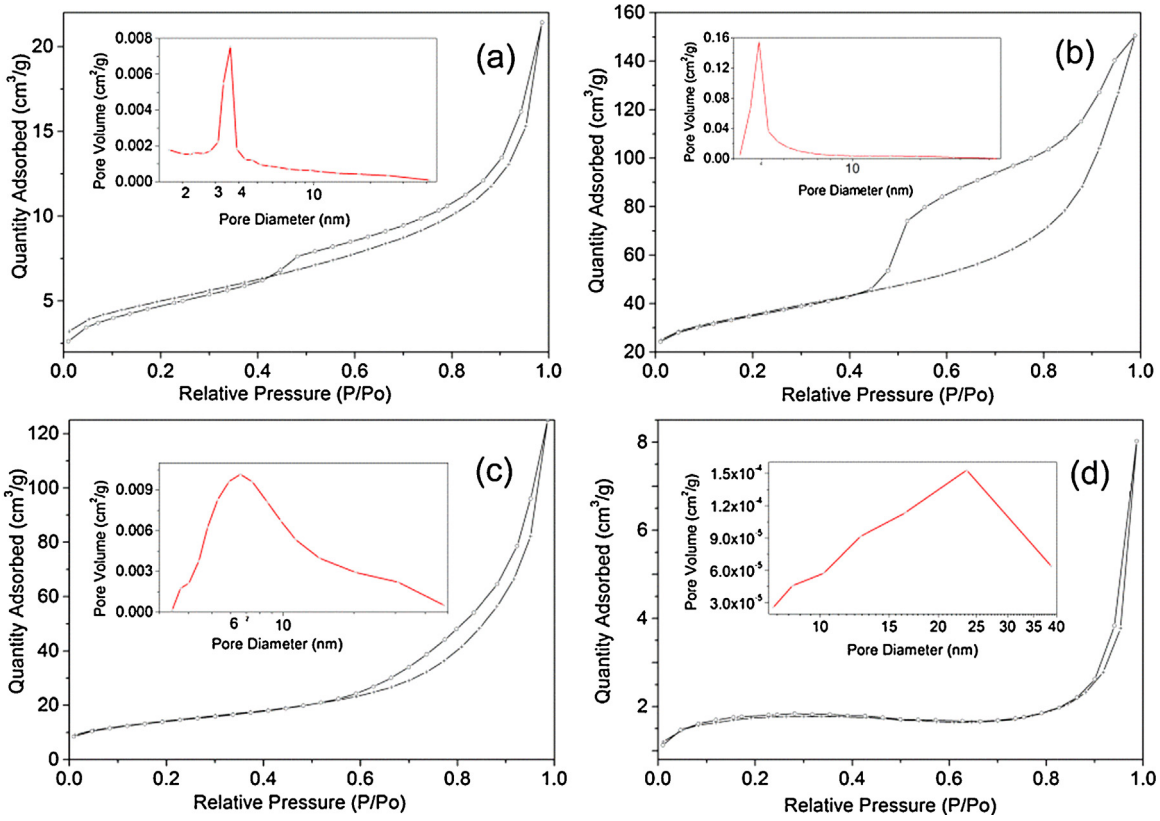

Fig. 2. Nitrogen adsorption/desorption isotherms of $MnFe_2O_4$ (a), $MnFe_2O_4$-SiC (b), $MnFe_2O_4$-TiO_2 (c) and $MnFe_2O_4$-diatomite (d).

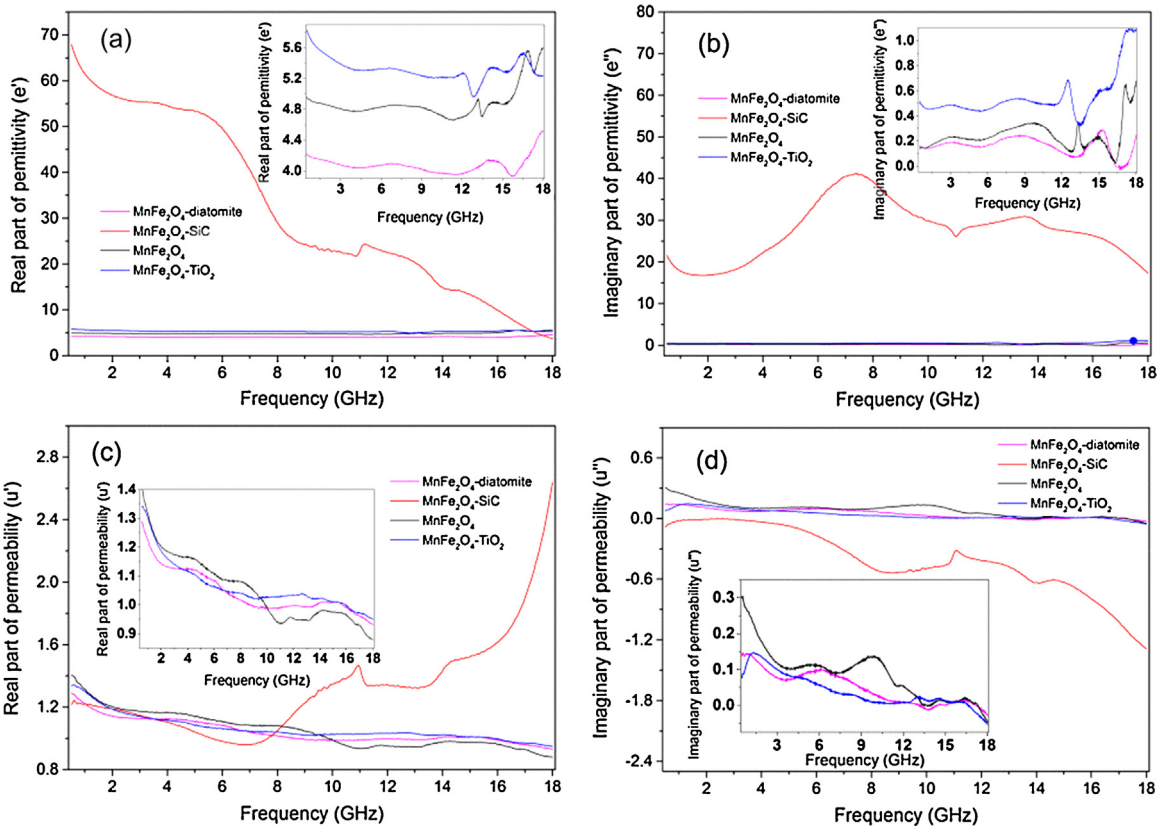

Fig. 3. The complex permittivity and complex permeability of $MnFe_2O_4$, $MnFe_2O_4$-SiC, $MnFe_2O_4$-TiO_2 and $MnFe_2O_4$-diatomite (a) real part of permittivity; (b) imaginary part of permittivity; (c) real part of permeability; (d) imaginary part of permeability.

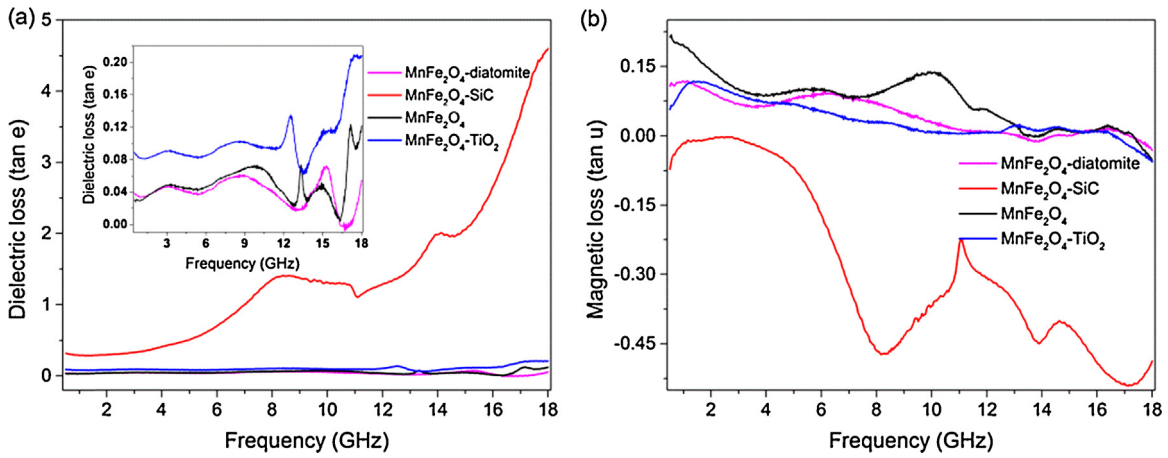

Fig. 4. Frequency dependence of the dielectric loss tangent (a) and magnetic loss tangent (b) of $MnFe_2O_4$, $MnFe_2O_4$-SiC, $MnFe_2O_4$-TiO_2 and $MnFe_2O_4$-diatomite.

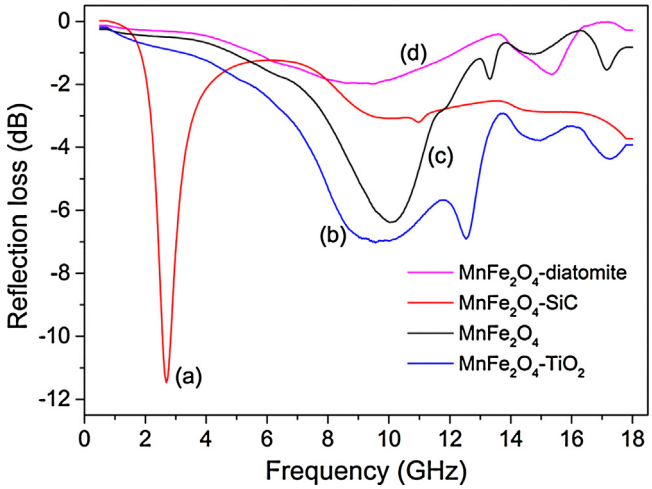

Fig. 5. Reflection loss of the four samples with the matching thickness of 3.5 mm.

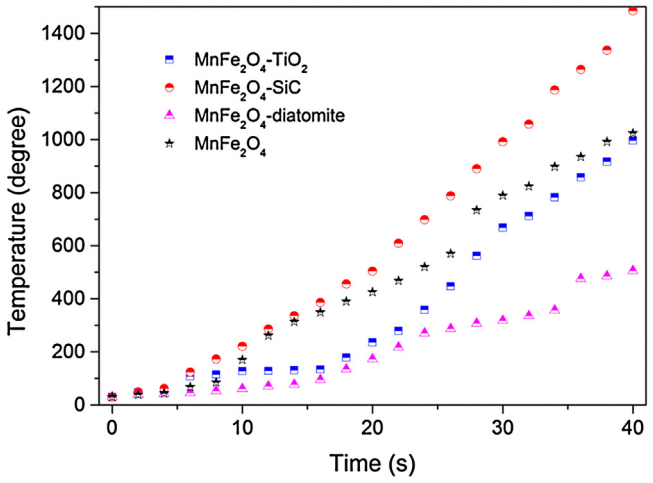

Fig. 6. The rising temperature curves of the four samples under microwave irradiation.

3.5. Surface temperature measurement

To measure the rising temperature of samples under microwave irradiation, the non-MW-absorbent quarts glass was selected as reactor. As shown in Fig. 6 the heating rate order of the four samples is $MnFe_2O_4$-SiC > $MnFe_2O_4$-TiO_2 > $MnFe_2O_4$ > $MnFe_2O_4$-diatomite. It was established that $MnFe_2O_4$-SiC could absorb MW energy strongly, exceeding 1450 °C within 40 s, which was higher than $MnFe_2O_4$-TiO_2 (1000 °C). On the other hand, the temperature of $MnFe_2O_4$-diatomite rose slowly and reached only 560 °C, which was even lower than that of the pure $MnFe_2O_4$. The differences in temperature measurement in the four samples stem from their different dielectric properties, which determine the ability to convert electromagnetic energy to thermal energy [35].

3.6. Microwave assisted catalytic degradation of RBR X-3B

To confirm the assumption that $MnFe_2O_4$-SiC has the stronger MW absorbing ability among the four catalysts, experiments on degradation of RBR X-3B were carried out under MW assisted conditions. The results are illustrated in Fig. 7. It can be seen that the $MnFe_2O_4$-SiC catalyst showed higher RBR X-3B degradation and TOC removal than the other three catalysts. After 5 min of irradiation, residual RBR X-3B concentration ratio decreased from 100% to 8%, 23%, 75% and 80%, respectively, when $MnFe_2O_4$-SiC, $MnFe_2O_4$-TiO_2, $MnFe_2O_4$-diatomite and pure $MnFe_2O_4$ were used in degradation. These values suggest that SiC, known as the perfect absorbent, accelerated the degradation and played a significant role in the degradation process. Hydrogen abstraction occurred at the metal surface of the exposed metal area and the elementary chain reactions that followed were the key factors which affected the activity of catalyst [36]. Herein, the interactions between $MnFe_2O_4$ and SiC could lead to higher catalytic activity and better RBR X-3B removal [37–39]. The higher MW absorbing property of $MnFe_2O_4$-SiC promotes faster and more efficient interactions between MW and catalysts. The reflection loss of $MnFe_2O_4$-SiC (over −10 dB) is the highest among the four catalysts at the frequency of 2.45 GHz. Therefore, almost all the microwave power (more than 90%) had been transferred to the surface of $MnFe_2O_4$-SiC, accelerating the degradation of RBR X-3B. On the contrary, a lower RBR X-3B removal is achieved by the $MnFe_2O_4$-diatomite which is a poorer MW absorbent.

A similar trend appeared in TOC removal. In Fig. 7(b), when $MnFe_2O_4$-SiC, $MnFe_2O_4$-TiO_2, $MnFe_2O_4$-diatomite and pure $MnFe_2O_4$ were added, TOC removal was 70%, 45%, 20% and 14%, respectively. After microwave-assisted catalytic reaction, the target compounds were degraded to be some inorganic carbon compounds in the liquid phase (see Fig. S2), contributing to the difference between TOC and removal. Interestingly, RBR X-3B was mostly mineralized by $MnFe_2O_4$-SiC, while the TOC removal with $MnFe_2O_4$-diatomite was much lower than that achieved with the other two catalysts. It is partly because that a lower adsorption RBR

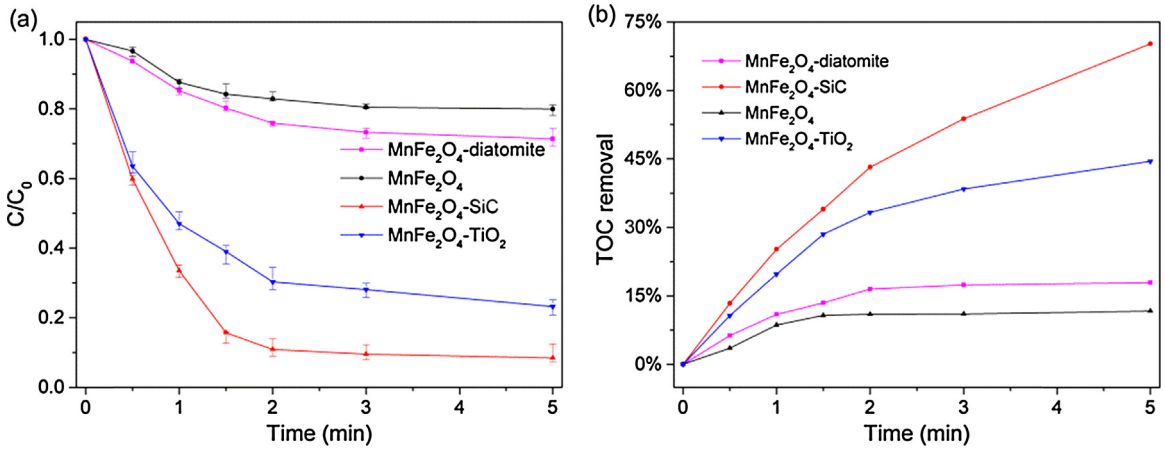

Fig. 7. Comparison of the four samples for the degradation (a) and TOC removal (b) under irradiation ([RBR X-3B] = 20 mg L^{-1}; [catalyst] = 1.5 g L^{-1}).

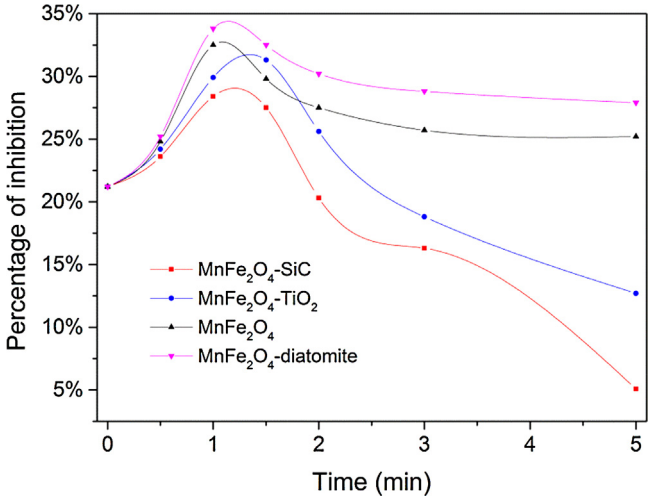

Fig. 8. Percentage inhibition after 30 min incubation of *Photobacterium phosphoreum* in RBR X-3B azo-dyes ([RBR X-3B] = 20 mg L^{-1}; [catalyst] = 1.5 g L^{-1}).

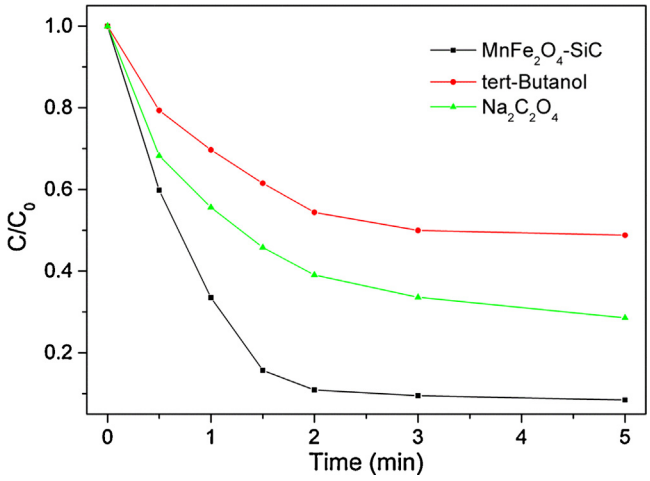

Fig. 9. Effects of various active oxygen species.

X-3B presented on its particle surface and the MW energy absorbed was lower. Given that the surface of $MnFe_2O_4$-SiC reached high temperature in a short time, it is safe to conclude that target compounds can be completely combusted [40], which facilitates higher degradation and mineralization of RBR X-3B. Therefore, RXR X-3B could be easily degraded under MW irradiation on the surface of $MnFe_2O_4$-SiC due to its admirable MW absorbing properties.

3.7. Microtoxicity

Relevant measurements were conducted to further evaluate the microtoxicity of the products obtained during degradation. Bioluminescence assay is a technique widely used for estimating wastewater toxicity or as a part of environment assessments. In this study, the results in the test solutions are presented in Fig. 8. The increase in toxicity between 0 and 1 min of irradiation with catalysts can be observed clearly. It may be attributed to the formation of highly toxic intermediates, namely inorganic carbon compounds produced in the liquid phase during the early stages of reaction [41–43]. However, it was noted that when $MnFe_2O_4$-SiC, $MnFe_2O_4$-TiO_2, $MnFe_2O_4$-diatomite and $MnFe_2O_4$ were added, the maximal inhibition was 28.4%, 31.3%, 33.8% and 32.5%, respectively. Higher inhibition demonstrates either the presence of highly toxic intermediates or incomplete degradation. Furthermore, the inhibition of samples after 1 min treatment slowed down, indicating the disappearance of the hazardous intermediates formed in the early stages of reaction. With 5% of inhibition after 5 min treatment, $MnFe_2O_4$-SiC was demonstrated to be an interesting catalyst with relatively lower toxicity of RBR X-3B during the reaction.

3.8. Possible mechanism on the catalytic degradation

To verify the main active oxygen species, two radical scavengers were added in the degradation (Fig. 9). In the presence of tert-butyl alcohol or $Na_2C_2O_4$, the degradation was apparently inhibited, indicating that hydroxyl radicals and superoxide anions were the significant species produced in the degradation.

The different catalytic performances could be viewed clearly when the four catalysts were added. Apparently, the support can be of great importance to the catalytic activity of the composites. Among the four composites, SiC coated $MnFe_2O_4$ performed the better degradation efficiency of RBR X-3B in the MW assisted system. It is noted that the $MnFe_2O_4$-SiC displayed higher activity than the pure $MnFe_2O_4$ alone. Silicon carbide (SiC), which is referred to as the notable dielectric, could strongly absorb the MW energy (see Fig. 10). Meanwhile, the energy could be quickly transferred to the nano-$MnFe_2O_4$ particles which were supported on the surface of SiC. Consequently, the surface temperature of the composites could rise rapidly, followed by the generations of many “hot spots”. Furthermore, the nano $MnFe_2O_4$-SiC composites exhibited the smaller size and larger surface, resulting in the significant increase and hypodispersion of “hot spots”. The temperature of “hot spots” in the water can exceed to 1000 °C or more, leading to the numerous

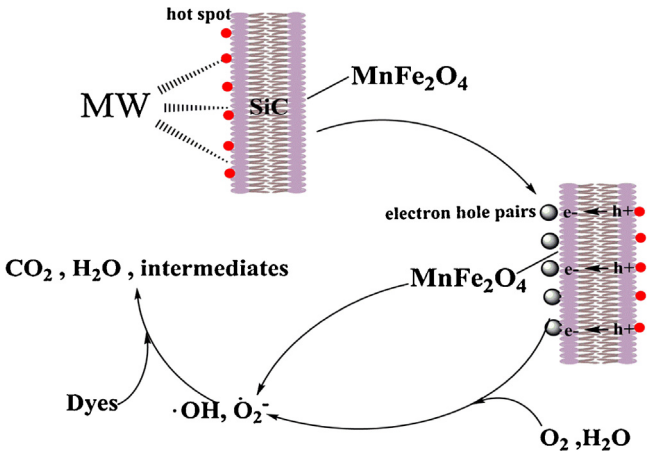

Fig. 10. Possible mechanism on degradation.

activated sits and holes [44]. Herein, the electron hole pairs can be generated to react with O_2 and H_2O to form the various active species, e.g. hydroxyl radicals or superoxide radical anion [15,45]. Furthermore, under MW irradiation, $O_2^{\bullet-}$ which comes from the lattice oxygen of $MnFe_2O_4$ could be produced to participate in the degradation of RBR X-3B [15]. Thus, the MW degradation process of pollutants, like RBR X-3B, could be enhanced significantly. Briefly, $MnFe_2O_4$-SiC can be a promising catalyst to generate much active radicals under MW irradiation, which is considered to enhance the degradation efficiency of pollutant.

4. Conclusion

Four typical catalysts have been synthesized successfully and their absorbing performances depending on the permeability and permittivity have been compared and discussed. The MW absorbing properties of composites are strongly influenced by the different supports introduced. $MnFe_2O_4$-SiC has demonstrated to be a novel and most efficient catalyst in MW assisted degradation when more active species, such as hydroxyl radicals and superoxide anions were produced. Interestingly, it showed remarkable RBR X-3B degradation efficiency of 92% and 70% TOC removal. Moreover, the toxicity of solution is relatively lower when $MnFe_2O_4$-SiC is employed, confirming the chains of characterization analysis according which $MnFe_2O_4$-SiC possessed superb MW absorbing properties. In conclusion, the microwave assisted degradation with $MnFe_2O_4$-SiC catalyst has demonstrated great potential for application in wastewater treatment.

Acknowledgements

The work was supported jointly by the National Natural Science Foundation of China (Grant No. 51278242) and Supporting project of Science and Technology in Jiangsu Province (BE2012116).

Appendix A. Supplementary data

Supplementary material related to this article can be found, in the online version, at http://dx.doi.org/10.1016/j.apcatb.2014.07.022.

References

[1] K. Esquivel, R. Nava, A. Zamudio-Mendez, M. Vega Gonzalez, O.E. Jaime-Acuna, L. Escobar-Alarcon, J.M. Peralta-Hernandez, B. Pawelec, J.L.G. Fierro, Appl. Catal. B 140 (2013) 213–224.
[2] S. Horikoshi, A. Osawa, S. Sakamoto, N. Serpone, Appl. Catal. A 460 (2013) 52–60.
[3] B. Maté, R.D. Suenram, C. Lugez, J. Chem. Phys. 113 (2000) 192–199.
[4] S. Horikoshi, H. Hidaka, N. Serpone, Environ. Sci. Technol. 36 (2002) 1357–1366.
[5] S. Horikoshi, A. Matsubara, S. Takayama, M. Sato, F. Sakai, M. Kajitani, M. Abe, N. Serpone, Appl. Catal. B 99 (2010) 490–495.
[6] T.-L. Lai, C.-C. Lee, G.-L. Huang, Y.-Y. Shu, C.-B. Wang, Appl. Catal. B 78 (2008) 151–157.
[7] Z. Zhang, Y. Shan, J. Wang, H. Ling, S. Zang, W. Gao, Z. Zhao, H. Zhang, J. Hazard. Mater. 147 (2007) 325–333.
[8] X. Zhang, Y. Wang, G. Li, J. Qu, J. Hazard. Mater. 134 (2006) 183–189.
[9] A.K.L. Sajjad, S. Shamaila, B. Tian, F. Chen, J. Zhang, J. Hazard. Mater. 177 (2010) 781–791.
[10] F. Han, V.S.R. Kambala, M. Srinivasan, D. Rajarathnam, R. Naidu, Appl. Catal. A 359 (2009) 25–40.
[11] E. Thostenson, T.-W. Chou, Composites Part A 30 (1999) 1055–1071.
[12] X. Quan, X. Liu, L. Bo, S. Chen, Y. Zhao, X. Cui, Water Res. 38 (2004) 4484–4490.
[13] J. Atwater, R. Wheeler Jr., Appl. Phys. A 79 (2004) 125–129.
[14] T.-L. Lai, C.-C. Lee, K.-S. Wu, Y.-Y. Shu, C.-B. Wang, Appl. Catal. B 68 (2006) 147–153.
[15] L. Zhang, X. Liu, X. Guo, M. Su, T. Xu, X. Song, Chem. Eng. J. 173 (2011) 737–742.
[16] Y. Wu, P. Qiao, J. Qiu, T. Chong, T.-S. Low, Nano Lett. 2 (2002) 161–164.
[17] H. Lin, H. Zhu, H. Guo, L. Yu, Mater. Lett. 61 (2007) 3547–3550.
[18] L. Olmedo, P. Hourquebie, F. Jousse, Adv. Mater. 5 (1993) 373–377.
[19] V. Petrov, V. Gagulin, Inorg. Mater. 37 (2001) 93–98.
[20] S. Sun, H. Zeng, D.B. Robinson, S. Raoux, P.M. Rice, S.X. Wang, G. Li, J. Am. Chem. Soc. 126 (2004) 273–279.
[21] D. Jones, T. Lelyveld, S. Mavrofidis, S. Kingman, N. Miles, Resour. Conserv. Recycl. 34 (2002) 75–90.
[22] A. de la Hoz, A. Diaz-Ortiz, A. Moreno, Chem. Soc. Rev. 34 (2005) 164–178.
[23] S. Hashemian, Main Group Chem. 10 (2011) 105–114.
[24] H.-M. Xiao, X.-M. Liu, S.-Y. Fu, Compos. Sci. Technol. 66 (2006) 2003–2008.
[25] Q. Su, J. Li, G. Zhong, G. Du, B. Xu, J. Phys. Chem. C 115 (2011) 1838–1842.
[26] L. Bo, Y. Zhang, X. Quan, B. Zhao, J. Hazard. Mater. 153 (2008) 1201–1206.
[27] M. Khadhraoui, H. Trabelsi, M. Ksibi, S. Bouguerra, B. Elleuch, J. Hazard. Mater. 161 (2009) 974–981.
[28] M. Neamtu, A. Yediler, I. Siminiceanu, A. Kettrup, J. Photochem. Photobiol. A: Chem. 161 (2003) 87–93.
[29] Y. He, L. Huang, J.-S. Cai, X.-M. Zheng, S.-G. Sun, Electrochim. Acta 55 (2010) 1140–1144.
[30] X. Hu, B. Liu, Y. Deng, H. Chen, S. Luo, C. Sun, P. Yang, S. Yang, Appl. Catal. B 107 (2011) 274–283.
[31] S. Yuan, P. Mériaudeau, V. Perrichon, Appl. Catal. B 3 (1994) 319–333.
[32] Z. Ai, Y. Wang, M. Xiao, L. Zhang, J. Qiu, J. Phys. Chem. C 112 (2008) 9847–9853.
[33] S.-S. Kim, S.-T. Kim, Y.-C. Yoon, K.-S. Lee, J. Appl. Phys. 97 (2005), 10F905-1–10F905-3.
[34] J. Huo, L. Wang, H. Yu, J. Mater. Sci. 44 (2009) 3917–3927.
[35] J. Menéndez, E. Menéndez, A. Garcia, J. Parra, J. Pis, J. Microw. Power Electromagn. Energy 34 (1999) 137–143.
[36] H. Gomes, J. Figueiredo, J. Faria, P. Serp, P. Kalck, J. Mol. Catal. A: Chem. 182 (2002) 47–60.
[37] A.S. Ivanova, E.M. Slavinskaya, R.V. Gulyaev, V.I. Zaikovskii, O.A. Stonkus, I.G. Danilova, L.M. Plyasova, I.A. Polukhina, A.I. Boronin, Appl. Catal. B 97 (2010) 57–71.
[38] Y. Wei, Z. Zhao, T. Li, J. Liu, A. Duan, G. Jiang, Appl. Catal. B 146 (2014) 57–70.
[39] Y. Yang, C. Ochoa-Hernandez, V.A. de la Pena O'Shea, P. Pizarro, J.M. Coronado, D.P. Serrano, Appl. Catal. B 145 (2014) 91–100.
[40] G. Deiber, J. Foussard, H. Debellefontaine, Environ. Pollut. 96 (1997) 311–319.
[41] A. Gottlieb, C. Shaw, A. Smith, A. Wheatley, S. Forsythe, J. Biotechnol. 101 (2003) 49–56.
[42] C. Wang, A. Yediler, D. Lienert, Z. Wang, A. Kettrup, Chemosphere 52 (2003) 1225–1232.
[43] M. Neamtu, C. Zaharia, C. Catrinescu, A. Yediler, M. Macoveanu, A. Kettrup, Appl. Catal. B 48 (2004) 287–294.
[44] Y. Chen, Z. Ai, L. Zhang, J. Hazard. Mater. 235 (2012) 92–100.
[45] Z. Zhang, Y. Xu, X. Ma, F. Li, D. Liu, Z. Chen, F. Zhang, D.D. Dionysiou, J. Hazard. Mater. 209 (2012) 271–277.